energies

MDPI

Article

# Numerical and Experimental Analysis of the Thermal Performances of SiC/Water and $Al_2O_3$/Water Nanofluid Inside a Circular Tube with Constant-Increased-PR Twisted Tape

**Saadah Ahmad [1,*], Shahrir Abdullah [1] and Kamaruzzaman Sopian [2]**

[1] Faculty of Engineering and Built Environment, National University of Malaysia, Bangi 43600 UKM, Malaysia; shahrir@ukm.edu.my

[2] Solar Energy Research Institute (SERI), National University of Malaysia, Bangi 43600 UKM, Malaysia; ksopian@ukm.edu.my

* Correspondence: saadah.a.sowi@gmail.com

Received: 11 March 2020; Accepted: 20 April 2020; Published: 22 April 2020


**Abstract:** The simultaneous use of two passive methods (twisted tape and a nanofluid) in a heat transfer system will increase the average Nusselt number (*Nu*) of the system. However, the presence of inserts and nanoparticles inside the tube will create higher pressure drop ($\Delta P$) in the system, which can eventually affect the overall enhancement ratio ($\eta$), especially at higher Reynolds numbers (*Re*). Several modifications of twisted tapes have been made to reduce $\Delta P$, but most showed a decreasing trend of $\eta$ as *Re* increased. The objective of this study is to design a new geometry of twisted tape that yields a larger value of *Nu* and a smaller value of $\Delta P$, which can result in a larger value of $\eta$ especially at higher *Re*. A simulation and experimental analysis are conducted in which *Re* ranges from 4000–16,000 with two types of nanofluids (SiC/Water and $Al_2O_3$/Water) at various values of the volume fraction, ($\varphi$) (1–3%). ANSYS FLUENT software with the RNG k-ε turbulent model is adopted for the simulation analysis. Three types of twisted tape are used in the analysis: classic twisted tape with a pitch ratio of 2 (TT PR2), constant-increasing-pitch-ratio twisted tape (TT IPR) and constant-decreasing-pitch-ratio twisted tape (TT DPR). The use of TT IPR generates a stronger swirling flow at the inlet of the tube and smaller $\Delta P$, especially near the outlet region. The highest value of $\eta$ is obtained for 3% SiC/Water nanofluid that is flowing through a smooth circular tube with TT IPR inserts at *Re* of 10,000.

**Keywords:** twisted tape; inserts; nanofluid; heat transfer; thermal performance

## 1. Introduction

The use of heat exchangers in industrial applications consumes an undesirable amount of energy and has become a matter of concern, especially in the effort to reduce energy waste, which can lead to climate change. Thus, increasing *Nu* and reducing $\Delta P$ are highly important for the realization of a higher performance heat exchanger. An approach for increasing the thermal performance of a thermal system is to adopt a passive method, such as alteration of the fluid flow inside a tube including having a corrugated channel/tube or using insert inside the channel/tube [1,2]. Therefore, several modifications have been made to the twisted tape by researchers to produce better fluid mixing with lower $\Delta P$ including serrated twisted tape (TPP) [3], multiple twisted tape [4], square and V-cut twisted tape [5], segmented twisted tape [6], and self-rotating twisted tape [7]. Even though all these methods are able to enhance $\eta$ at a certain point, a decreasing trend is shown as *Re* increases. Another promising passive method that can be applied in the effort of increasing thermal performance in heat exchanger

systems is using nanofluid as the working fluid. The simultaneous use of these two methods will result in higher *Nu* but at the expense of higher $\Delta P$ due to flow blockage by the twisted tape insert and higher viscosity of the fluid due to nanoparticles.

These modified approaches include a cross-cut twisted tape with an alternate axis (CCTA) with a Cu/Water nanofluid as the working fluid [8,9], twin co-twisted tapes and twin counter-twisted tapes (CoTs and CTs) with a graphene-platinum nanofluid as the working fluid [10], overlapped dual twisted tapes (O-Dts) with a TiO2/Water nanofluid as the working fluid [11], helical twisted tape with an $Al_2O_3$/ water nanofluid as the working fluid [12], twisted tape with dimples and protrusions with an $Al_2O_3$/Water nanofluid as the working fluid [13], dual co-twisted tapes and dual counter-twisted tapes (D-Co-TTs and D-C-TTs) with an $Al_2O_3$/Water nanofluid as the working fluid [14], rectangular-cut-on-its-rib twisted tape with four types of nanofluids as working fluids ($TiO_2$/Water, BeO/Water, ZnO/Water, and CuO/Water) [15], twisted tapes with various progression ratios (RGPR and IGPR) with an $Al_2O_3$/Water nanofluid as the working fluid [16], spiky twisted tape with three types of nanofluids as the working fluid (Cu/Water, Fe/Water, and Ag/Water) [17], and trapezoidally cut twisted tape with an $Fe_3O_4$/Water nanofluid as the working fluid [18]. The simultaneous use of these two passive methods increased $\eta$ by a factor 1.2–1.5 for *Re* between 4000–10,000 compared to classic twisted tape with water as the working fluid. The utilization of multiple twisted tapes such as O-Dts and D-Co-TT can create a stronger swirling flow inside the tube that results in higher *Nu*. However, multiple twisted tapes yielded 20% higher pressure drop and pumping power compared to the classic single twisted tape under the same PR condition due to the additional contact surface between the working fluid and the inserts [10]. Modifications to a single twisted tape, such as perforation, notching and jagged cutting, have been made by Rahimi et al. [19]. Numerical and experimental analyses have been conducted to select the best modification of the twisted tape. According to the results, jagged twisted tape yielded the largest value of $\eta$, followed by classic, notched and perforated twisted tapes. Even though the classic twisted tape yielded the strongest swirl flow among the modifications, the jagged twisted tape created a higher turbulence intensity field, especially at the jagged edge region, which led to better fluid mixing and higher *Nu*.

Most of the available modifications to the twisted tape yielded larger values of $\eta$ than that of the classic twisted tape but showed a decreasing trend in $\eta$ as *Re* increased. Tabatabaeikia, et al. [20], however, found out that perforated twisted tape and notched twisted tape do not give much difference in Overall Enhancement Ratio ($\eta$) as compared to other modifications. Eiamsa-ard et al. [21] investigated the effect of modified twisted tape with triangle/rectangular/trapezoidal wings (O- Tri/O-Rec/O-Tra/P-Tri/P-Rec/P-Tra) on heat transfer (*h)*, friction factor (*f)* and Overall Enhancement Ratio ($\eta$). The result shows that the modified twisted tapes give higher $\eta$ compared to classic twisted tape. Khoshvaght-Aliabadi and Eskandari [22] conducted an experimental analysis on the overall performance of a low-to-high twisted tape insert with a Cu/Water nanofluid. The results demonstrated that the low-to-high PR twisted tape yielded an increasing trend of $\eta$ as *Re* increased. However, the maximum $\eta$ value of the low-to-high twisted tape was lower than those of other modifications, such as RGPR and rotation of the twisted tape [23]. This is due to differences in terms of other parameters that influenced the system's performance.

In addition to the modification of the twisted tape, the type, size, shape and volume fraction of the nanoparticles are important parameters for heat transfer augmentation [24]. Due to superior thermophysical properties, such as thermal conductivity ($k$), specific heat ($c_p$), density ($\rho$) and viscosity ($\mu$), a nanofluid is a superior substitute as a working fluid. However, similar to the inserts (twisted tape), the addition of nanoparticles into the system caused a higher $\Delta P$ due to the higher viscosity of the fluid [25]. Therefore, the selection of a suitable value of $\varphi$ is important for ensuring that larger $\eta$ is realized [26].Due to that, further exploration and analysis are necessary of the type of nanofluid and the value of $\varphi$ that can result in an increasing value of $\eta$ as *Re* increases. Vajjha and Das [27] analyzed the effects of three types of nanofluids (CuO, $Al_2O_3$ and $SiO_2$) on the pumping power of a system. All types of nanofluids required less pumping power than water at 2% of $\varphi$. However, at 43% of $\varphi$, the

CuO/Water nanofluid required more pumping power than water due to an additional pressure drop and higher fluid viscosity. Previous experimental and numerical studies were all carried out based constant PR twisted tape. Therefore, the effect of dynamic PR (different pitch ratio at inlet and outlet) towards improvement of $\eta$ was not studied. Therefore, the main aim of this technical study is to study the effect of dynamic PR on a given twisted tape arrangement towards the improvement of fluid flow, heat transfer, friction loss and ultimately $\eta$. Determining the most optimum nanofluid that works best with such configuration is also part of the study. So, the objective of the study is to investigate the turbulent forced convection flow of $Al_2O_3$/Water and SiC/Water at different $\varphi$ with two different types of modified twisted tape inserts: Increasing Pitch Ratio (IPR) and Decreasing Pitch Ratio (DPR). TT IPR and TT DPR are different from the classic twisted tape due to variation in PR from the inlet to the outlet. The effect of *Re*, φ and type of modified twisted tape to the *Nu*, *f* and $\eta$ will be analyzed numerically and experimentally. The analysis is conducted under constant wall heat flux with *Re* from 4000 to 16,000.

## 2. Materials and Methods

Research methods are comprising of two categories: numerical and experimental methods. The analysis was first conducted using numerical and later validated through experimental methods. Results from both methods are compared and analyzed.

### *2.1. Numerical Method*

The geometry and dimensions of the twisted tape are presented in Figure 1. The first geometry is classic TT with PR equal to 2, the second geometry is TT IPR with PR of 1.5 at the inlet and increasing by 0.25 towards the outlet, and the third geometry is TT DPR with PR of 6 at the inlet and decreasing by 0.25 towards the outlet. $Al_2O_3$/Water and SiC/Water nanofluids flow in a circular tube that is equipped with twisted tape for various values of $\varphi$ (1–3%). The full images of the test sections are illustrated in Figure 2. Table 1 presents the values of the defined parameters. Turbulent flow is chosen for the simulation analysis because it is more relevant to the practical scenario. The prediction of the turbulent flow model and the heat transfer behaviour are considered in the selection of the most relevant mathematical model. A simulation analysis is conducted using the ANSYS Fluent software 16.1 [28].

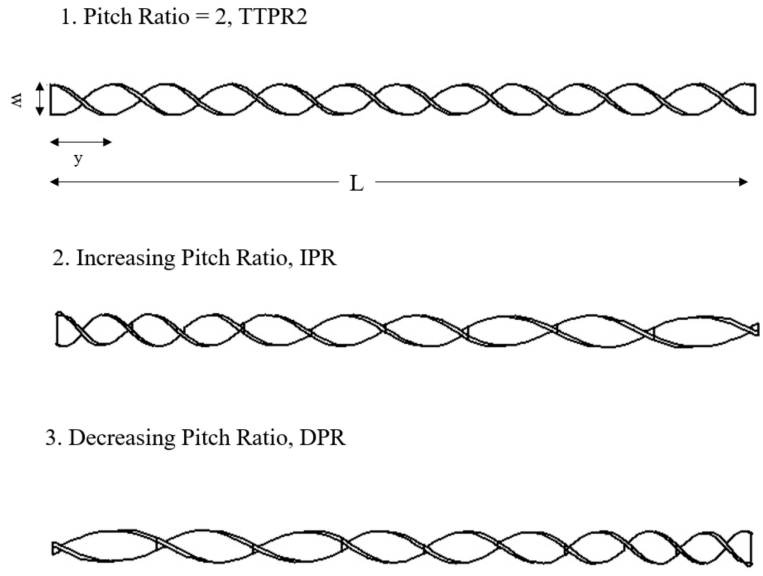


**Figure 1.** Geometries of the twisted tape.

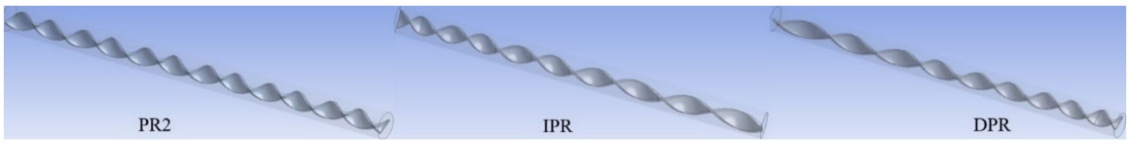


**Figure 2.** Smooth circular tube with twisted tape inserts.

**Table 1.** Parameter definitions.

| Parameter | Definition |
|---|---|
| D = 19 mm | Tube diameter |
| t = 1.9 mm | Twisted tape thickness |
| w = 12.7 mm | Tape width |
| L = 300 mm | Tube length |
| y | Pitch length |
| PR | Pitch ratio (y/w) |
| Re = 6000 – 14 000 | Reynolds number |
| $\varphi$ = 1%, 2% and 3% | Nanoparticle volume fraction |

#### 2.1.1. Simulation and Boundary Condition

The pressure-based finite volume method is used to conduct the simulation. The SIMPLE algorithm is used for velocity-pressure coupling [29]. To discretize the turbulent kinetic energy, the momentum, the turbulent dissipation rate, and the energy equations, the second-order upwind scheme is employed. The convergence criteria for the residues of the continuity, the momentum, the velocities, and the energy are set to $10^{-6}$. The $Al_2O_3$/Water and SiC/Water nanofluids enter the test section at an inlet temperature $T_{in}$, which is set to 300 K. For the inlet, the velocity-inlet condition is applied, while the pressure-outlet condition is applied at the outlet. The heat flux at the tube wall is maintained at a constant value of 1000 W/m$^2$.

#### 2.1.2. Governing Equations

Three Navier-Stokes equations for the swirl-dominant turbulent flow are solved: continuity, momentum and energy equations. The assumptions that were adopted in the modelling of the fluid flow and the heat transfer process inside the tube with twisted tape are steady 3-D flow, constant fluid properties, and neglect of the natural and thermal radiation. The twisted tape produced a swirl flow inside the tube. Hence, the RNG k-ε epsilon model with the enhanced wall treatment method is selected for the prediction of the turbulent flow characteristics inside the tube due its performance in analysing the small scale of the flow and the swirl-dominant flow with a reasonable computation time. The RNG k-ε model is derived from the instantaneous Navier Stokes equation via the "renormalized group" (RNG) method. Two transport equations for the turbulent model are as follows:

$$\frac{\partial}{\partial t}(\rho k) + \frac{\partial}{\partial x_i}(\rho k u_i) = \frac{\partial}{\partial x_i}\left(\alpha_k \mu_{eff} \frac{\partial k}{\partial x_j}\right) + G_k + G_b - \rho\epsilon - Y_M + S_k \quad (1)$$

$$\frac{\partial}{\partial t}(\rho \epsilon) + \frac{\partial}{\partial x_i}(\rho \epsilon u_i) = \frac{\partial}{\partial x_j}\left(\alpha_\epsilon \mu_{eff} \frac{\partial \epsilon}{\partial x_j}\right) + C_{1\epsilon}\frac{\epsilon}{k}(G_k + C_{3\epsilon}G_b) - C_{2\epsilon\rho}\frac{\epsilon^2}{k} - R_\epsilon + S_\epsilon \quad (2)$$

where $G_k$ denotes the generated turbulence kinetic energy that is due to the mean velocity gradients; $G_b$ denotes the generated turbulence kinetic energy that is due to the buoyancy; $Y_M$ denotes the contribution of the fluctuating dilatation in compressible turbulence to the overall dissipation rate; $\alpha_k$ and $\alpha_\epsilon$ are the inverse effective Prandtl numbers for k and ϵ, respectively; and $S_k$ and $S_\epsilon$ are user-defined source terms. The effective viscosity is expressed as

$$\mu_t = \rho C_\mu \frac{k^2}{\epsilon} \quad (3)$$

All the constant values for the transport equations are presented in Table 2. Although nanofluid is the mixture of nanoparticles and base fluid, which in general is a two-phase liquid, it is assumed that the nanoparticles can be easily fluidized and it is valid to be considered as a conventional single-phase (homogenous) fluid having average physical properties of individual phases [30,31]. The thermophysical properties of the nanofluid are calculated by employing a single-phase model assumption that neglects the temperature-dependence of thermophysical properties and nanoparticles Brownian motion [32]. The expressions of nanoparticles properties are as follows:

**Table 2.** Constant values of the transport equations.

| Constant | Value |
|---|---|
| $C_\mu$ | 0.0845 |
| $\sigma_k$ | 0.7194 |
| $\sigma_\epsilon$ | 0.7194 |
| $C_{\epsilon 1}$ | 1.42 |
| $C_{\epsilon 2}$ | 1.68 |
| $\eta_0$ | 4.38 |
| $\beta$ | 0.012 |

Density [33]:

$$\rho_{nf} = (1-\varphi)\rho_f + \varphi\rho_p \tag{4}$$

Specific heat [34]:

$$C_{p,nf} = \frac{(1-\varphi)\rho_f C_{p,f} + \varphi\rho_p C_{p,p}}{\rho_{nf}} \tag{5}$$

Viscosity [35]:

$$\mu_{nf} = \frac{\mu_f}{(1-\vartheta)^{2.5}} \tag{6}$$

Thermal conductivity [36]:

$$\frac{k_{nf}}{k_f} = \frac{k_p + 2k_f + 2\varphi\left(k_p - k_f\right)}{k_p + 2k_f - \varphi\left(k_p - k_f\right)} \tag{7}$$

$\frac{k_{nf}}{k_f}$ where $\varphi$ is the nanoparticle volume fraction (1%, 2% and 3%), and f and p denote fluid and particle, respectively.

#### 2.1.3. Mesh Generation

Figure 3 presents the generated mesh of the physical model, the twisted tape and the circular tube. Inflation-layer mesh control is applied at the tube wall to accurately simulate the boundary-layer region where the velocity and temperature are rapidly changing. Tetrahedral grids are used to generate the mesh at the tube wall due to the temperature–boundary–layer region. Fine mesh sizing is employed on the twisted tape to capture the narrow and curved regions of the tape. To ensure that the selected mesh does not depend on the cell size, a grid independence test is conducted using TTPR2 twisted inside a circular tube with water as the working fluid. Table 3 summarizes the values of *Nu* and ΔP that were obtained for four numbers of cells under the same simulation conditions. The main objectives of the test are to ensure that the selected grid mesh yields satisfactory accuracy within a reasonable computation time [13]. The results demonstrate that the differences in *Nu* and $\Delta P$ among the four selected grids are relatively small, namely, less than 1%. Even though a grid with 1,134,125 cells yields the largest values of *Nu* among the grids with the examined numbers of cells, it takes four times longer to converge than the grid with 519,393 cells. Hence, the grid with 519,393 cells is selected for simulation.

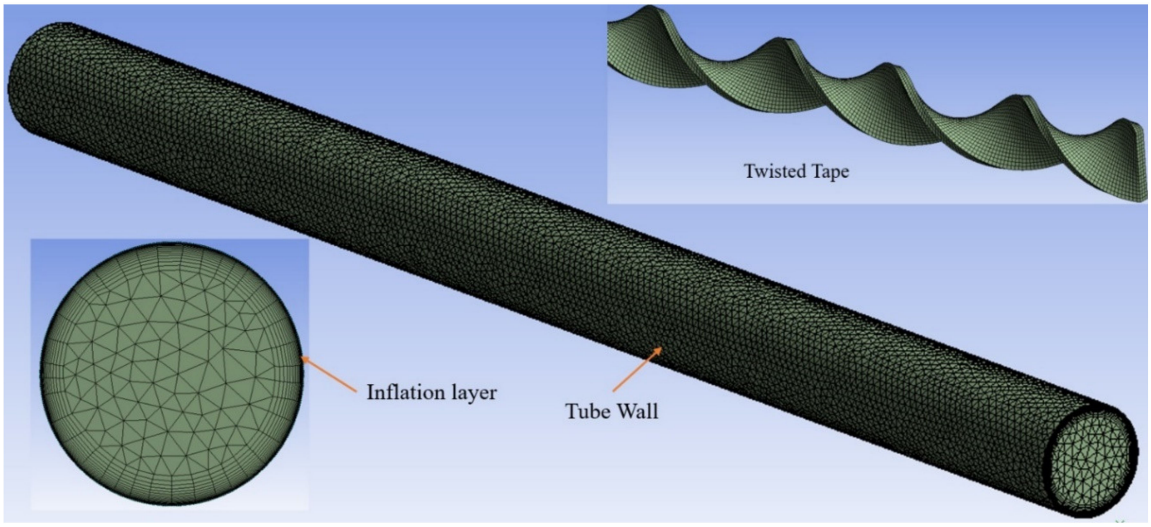


**Figure 3.** Mesh generation of a circular tube and twisted tape.

**Table 3.** Values of Nu and ΔP with four numbers of cells.

| Number of Cells | *Nu* | ΔP |
|---|---|---|
| 519,393 | 125.78 | 72.543 |
| 723,435 | 125.98 | 72.673 |
| 874,532 | 126.123 | 72.689 |
| 1,134,125 | 126.234 | 72.698 |

## 2.2. Experimental Method

### 2.2.1. Preparation and Characterization of Nanofluid

Two type of nanoparticles with the same diameter and shape are selected to produce nanofluid; SiC and $Al_2O_3$. Field Emission Scanning Electron Microscopy is used to check on the particles size and shape. Result showed that both SiC and $Al_2O_3$ nanoparticles are approximately circle with 40 nm diameter, which is in agreement with the datasheet from the supplier. Two-step method is used to produce nanofluid due to its lower cost and being more practical in producing a higher volume of nanofluid. The minimum amount of nanofluid that needs to be produced for one run of the experiment is 7 litres. Nanofluid is prepared by dispersing nanoparticles with the desired amount (1%, 2% and 3%) into distilled water (base fluid) by using sonication bath. The mixture is well homogenized at 120W, 40 kHz and 328 K with 2 hrs of sonication time. The stability of nanofluid is checked through visual inspection and viscosity measurement. After 24 h, there is no trace of sedimentation at the bottom of the SiC/Water and $Al_2O_3$/Water nanofluid (shown in Figures 4 and 5). Figure 6 shows the viscosity values for both SiC/Water and $Al_2O_3$/Water nanofluid after 1 h and 24 h of preparation at the same temperature (298 K). The difference in viscosity is very small (approximately 0.19% difference), hence the nanofluid is considered stable during the period the experiments are conducted (within 24 h). Thermal physical properties of nanofluid are characterised by measuring thermal conductivity (k), specific heat ($c_p$), viscosity (μ), and density (ρ). The equipment used to measure all the thermal physical properties are Kd2 Pro Thermal Properties Analyzer, Brookfield Rheometer DV3T-7 inch and electronic densimeter DH-300L (shown in Figure 7). The reading for each property is taken three times and the mean value is used for the analysis.

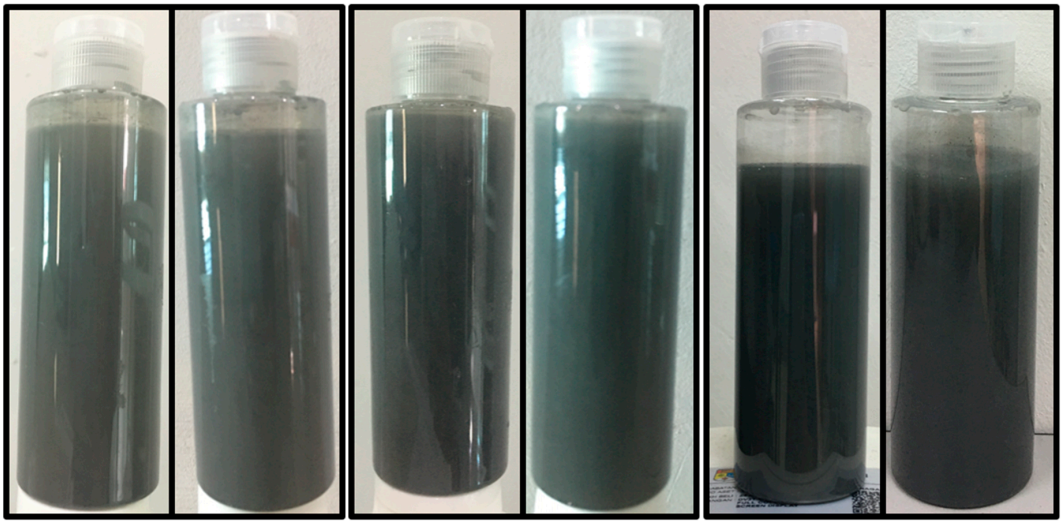


**Figure 4.** SiC/Water nanofluid at different φ.

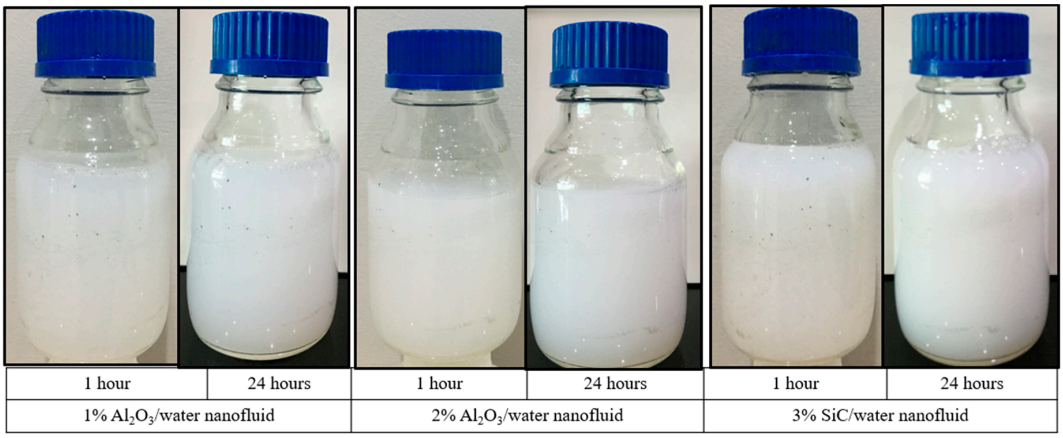


**Figure 5.** $Al_2O_3$/Water nanofluid at different φ.

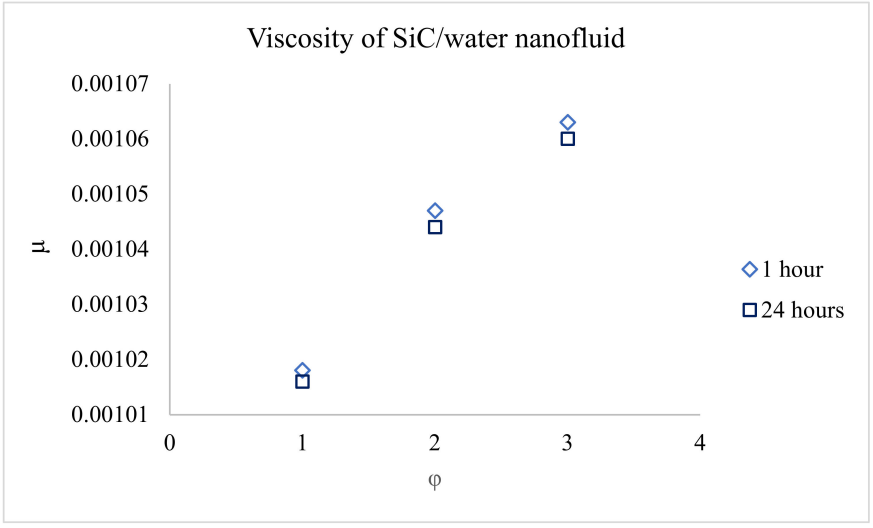


**Figure 6.** Comparison of viscosity values for SiC/Water nanofluid after 24 h of preparation.

**Figure 7.** Equipment for thermal physical characterization.

### 2.2.2. Experimental Setup

The schematic diagram of the experimental setup that consisted of a 1) heating loop, 2) cooling loop, 3) test section, and 4) twisted tape is shown in Figure 8. Nanofluid is flowing from the nanofluid tank at room temperature (~300K) through a flow meter (used to set the inlet velocity of the working fluid) into a copper tube. Pressure sensors and K-type thermocouples are inserted at the inlet and outlet of the copper tube to measure both the inlet and outlet pressure and temperature. From the test section, the heated nanofluid will flow through a heat exchanger to release the heat before flowing into the nanofluid tank, and the cycle continues. The experiment is set up in the Solar Energy Research Institute (SERI), UKM as shown in Figure 9.

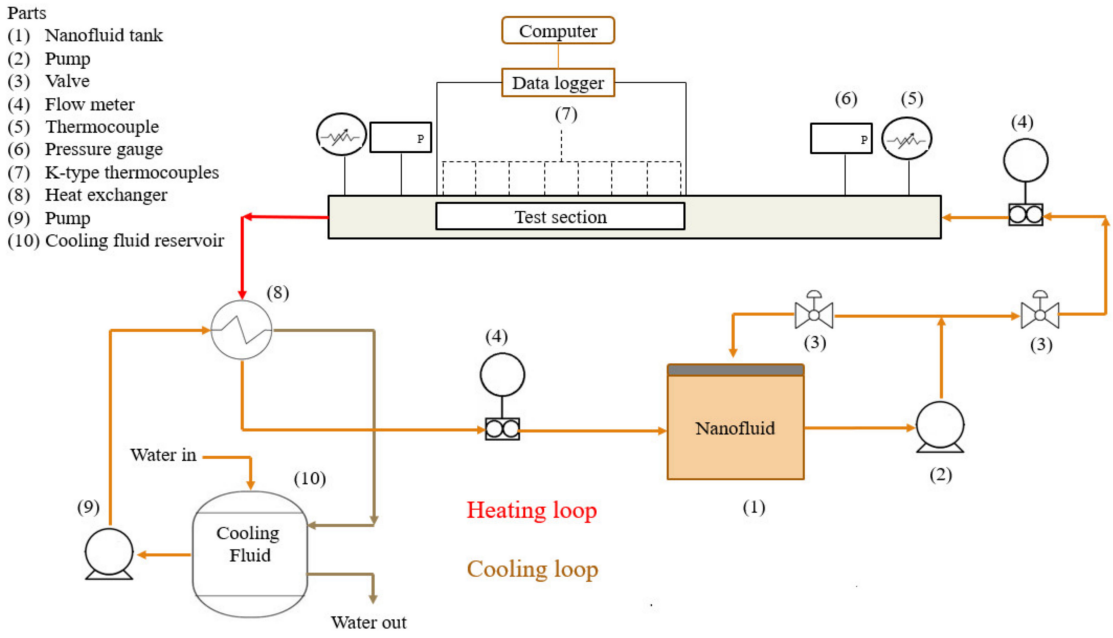


**Figure 8.** Schematic diagram of experimental set-up.

### 2.2.3. Test Section and Twisted Tape Geometry

The test section consisted of 1) a developing section, 2) eight thermocouples, 3) a silicone heater strip, 4) a voltage regulator, and 5) a power supply, as is shown in Figure 10. Four-hundred millimetres of the developing section is set prior to the inlet in order to make sure that the fully developed flow is entering the test section. A 1-meter silicone heater strip is rolled along the tube wall with a 19 mm inner diameter. At the tube wall, eight thermocouples are attached at constant distance by using thermal

epoxy. Voltage regulator and power supply are connected to the tube wall in order to keep the heat flux constant at 1000w/m$^2$ throughout the experiments. The test section is well insulated to make sure there is no heat lost during the experiment. Twisted tapes are made of straight aluminium bar with 18.5 mm width and 1 mm thickness, which have been manually twisted to the desired design. Figure 11 shows three different geometries of twisted tapes that are used for the experiments.

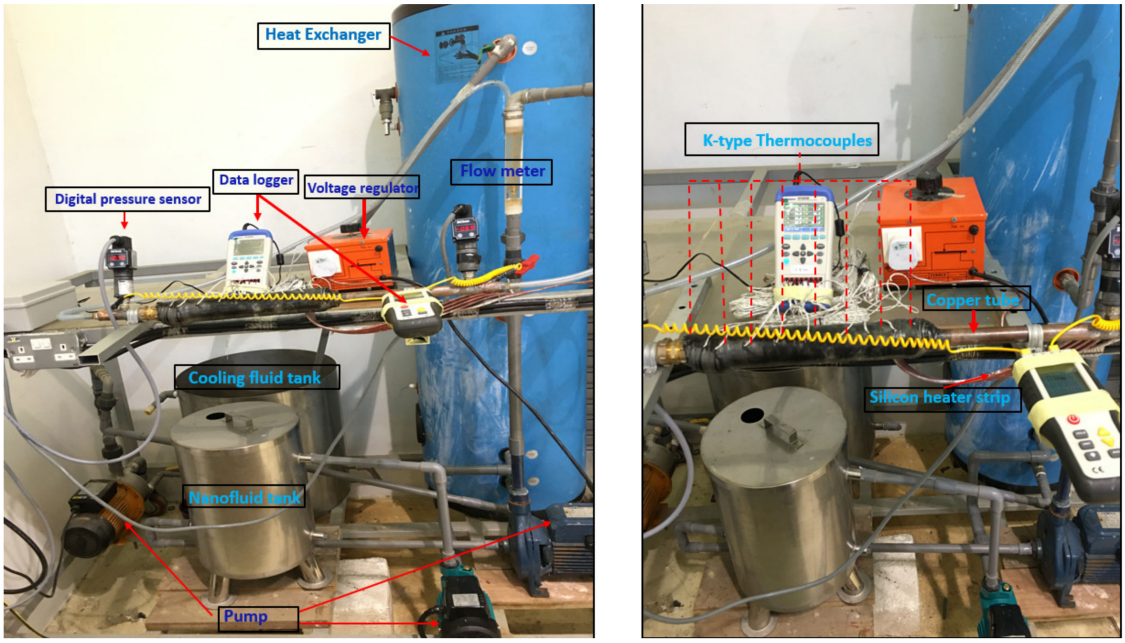


**Figure 9.** Experimental set-up.

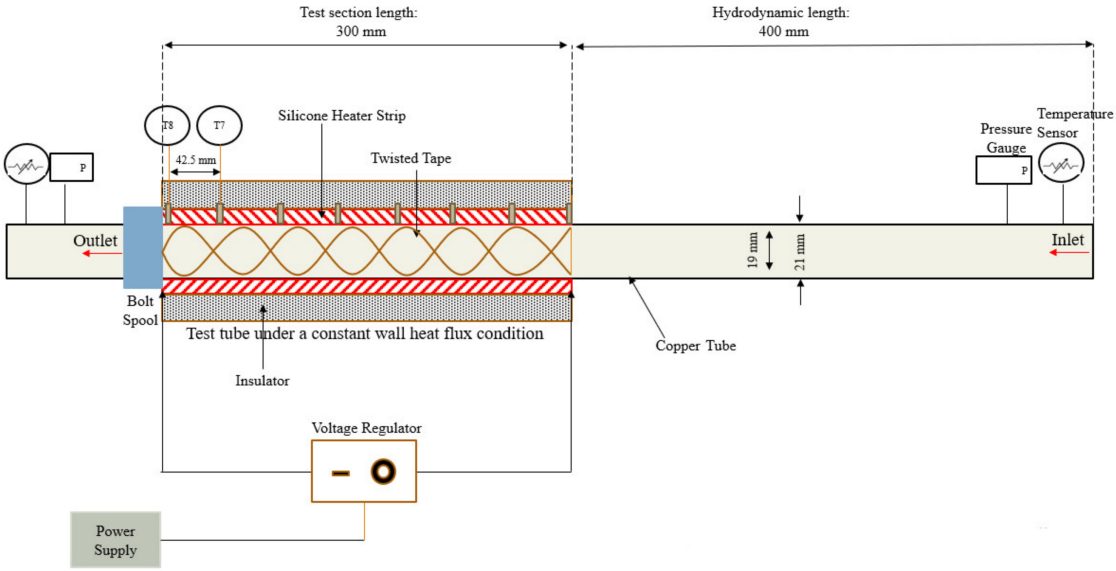


**Figure 10.** Schematic diagram of the test section.

## 2.3. Data Reduction

The heat transfer enhancement was calculated based on the following dimensionless parameters: Reynolds number:

$$Re = \frac{\rho u D}{\mu} \tag{8}$$

where u is the average fluid velocity in the tube

Friction factor:

$$f = \frac{2D\Delta P}{\rho L u^2} \tag{9}$$

Nusselt Number:

$$Nu = \frac{hD}{k} \tag{10}$$

By applying a constant-heat-flux condition at the tube wall, the convective heat transfer coefficient h is calculated as follows [37]:

$$h = \frac{q}{T_w - T_f} \tag{11}$$

where $T_w$ and $T_b$ denote the pipe wall temperature and the bulk temperature, respectively.

Overall enhancement ratio:

$$\frac{Nu/Nu_p}{(f/f_p)^{\frac{1}{3}}} \tag{12}$$

where $Nu_p$ and $f_p$ are the values of *Nu* and f, respectively, that are obtained for a plain circular tube with water.

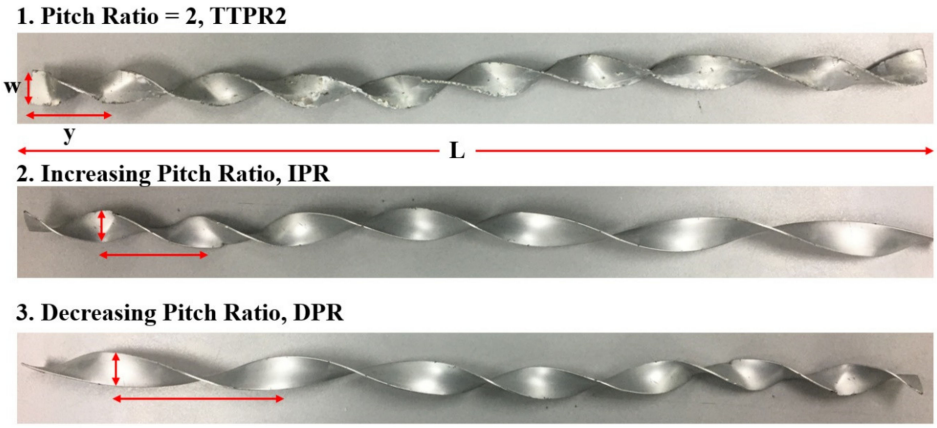


**Figure 11.** Geometries of twisted tape.

## 3. Results and Discussion

This section may be divided by subheadings. It should provide a concise and precise description of the experimental results, their interpretation as well as the experimental conclusions that can be drawn.

### *3.1. Evaluation*

The accuracy of the numerical and experimental analysis for a smooth tube with water flowing through the test section is evaluated based on the following values from the literature [38]: the Dittus-Boelter and Gnielinski correlations for *Nu* and the Pethukov correlations for the friction factor. According to Figure 12, the values for both *Nu* and *f* obtained from the present study are in accord with the values obtained from previous studies. There is an abrupt change in the slope of the *Nu* curve for the experimental result potentially due to data sampling and measurement errors. For instance, during the experimental run at high Reynolds Number, the setup was observed to be a bit unstable due to high vibration and digital sensor readings were impacted. The recorded measurements were highly dynamic at that time and it was challenging to extract the precise bulk temperatures. The accuracy of the numerical and experimental analysis for a tube that is equipped with a twisted tape is evaluated using experimental data from Eiamsa-ard and Kiatkittipong [39], Karami et al. [40], Naphon [41], Manglik and Bergles [42], and Ponnada et al. [43]. All the comparisons are conducted with a PR of 3 under a turbulent flow with Reynolds numbers from 4000 to 16,000. From Figure 13, the numerical results that are obtained for *Nu* show an average deviation of 10.5% compared to the experimental

data, with a similar increasing trend as *Re* increases. The deviation is due to experimental error, which mostly is contributed to by $T_{in}$ deviation between the numerical and experimental. Due to a deficiency in the experimental setup (i.e. the chiller was not installed to cool down the $T_{out}$ of fluid), $T_{in}$ was not able to be kept at room temperature of 300 K, hence causing the slight inaccuracy of the result. For *f*, the data that were obtained from the numerical and experimental results accord with those that were obtained by Eiamsa-ard and Kiatkittipong [39] and Naphon [41]. The significant difference in *f* values might be due to the difference in the thickness of the twisted tape, as some experimental analyses assumed a very small thickness of the twisted tape, while the actual thickness for the simulation is 1 mm. However, the graph shows similar decreasing trends as *Re* increases. *Nu* is increasing with *Re* due to the higher temperature gradients at the boundary layer of the tube. Moreover, *f* is inversely proportional to *Re* due to an increase in the tangential velocity, and the trends are similar to the Moody chart for turbulent flows. In addition, the $Y^+$ values are calculated and presented in Table 4 to provide a more accurate prediction of the flow field at the boundary layer, especially near the wall region, where the limit on $Y^+$ for k-ε with the enhanced wall treatment method should be less than 5.

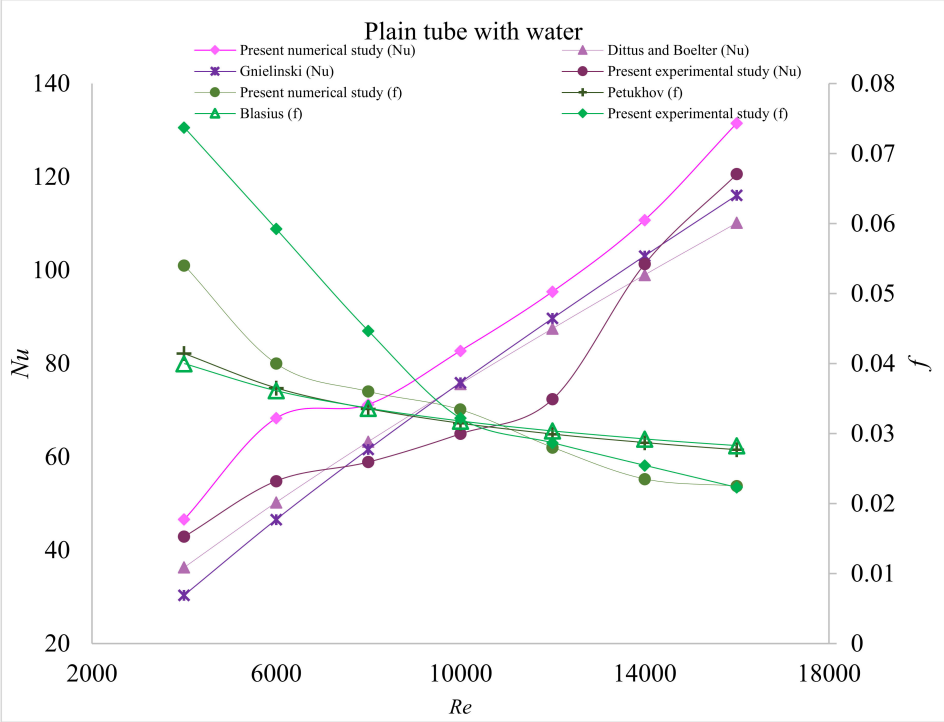


**Figure 12.** Validation of water flowing inside a smooth circular tube.

**Table 4.** Y+ values for various simulation conditions.

| Case | Type of TT | *Re* | $Y^+$ |
|---|---|---|---|
| 1 | PR2 | 4000 | 0.4940 |
| 2 | PR2 | 10,000 | 0.9483 |
| 3 | IPR | 4000 | 0.4579 |
| 4 | IPR | 10,000 | 0.8949 |
| 5 | DPR | 4000 | 0.6115 |
| 6 | DPR | 10,000 | 0.8724 |

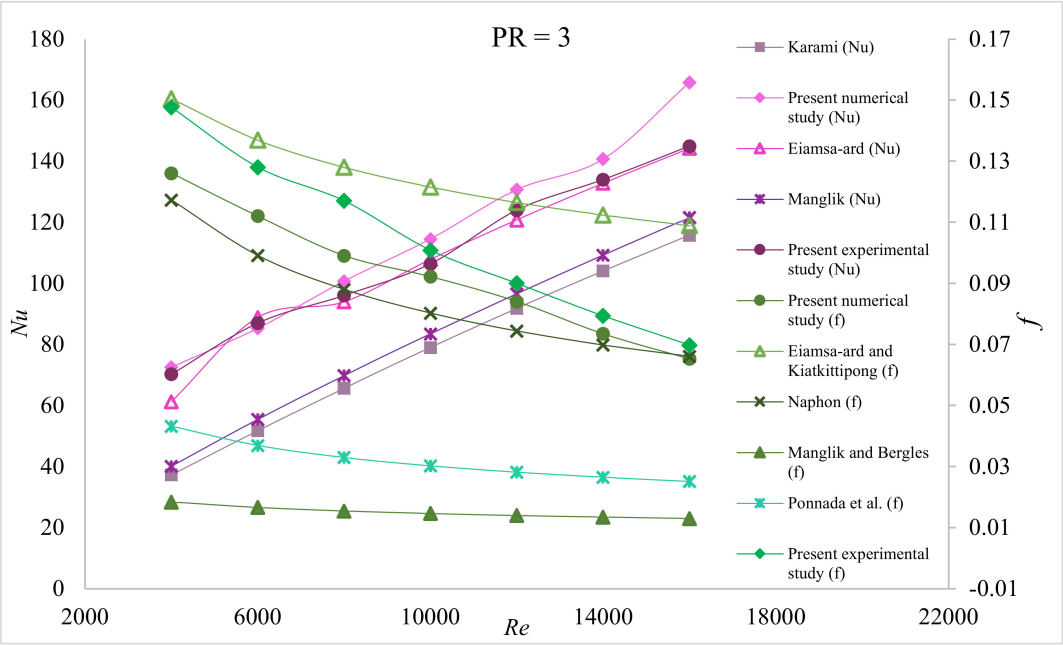


**Figure 13.** Validation of water flowing inside a circular tube with a twisted tape insert.

### 3.2. Uncertainties

In order to make sure that all instruments used for data measurement and experimental procedures are reliable and have a good accuracy, the calibration process is conducted prior to use. Dependent variables such as $Nu$, $f$, $Re$, and $\eta$ are influenced by independent variables such as temperature, local pressure and volumetric flow rate. Hence, the following equation is used [44] to measure the uncertainties of the experimental parameters.

$$\sigma_R = \pm\sqrt{\left(\frac{\partial R}{\partial x_1}\sigma_{x_1}\right)^2 + \left(\frac{\partial R}{\partial x_2}\sigma_{x_2}\right)^2 + \cdots + \left(\frac{\partial R}{\partial x_n}\sigma_{x_n}\right)^2}$$

where $\sigma_R$ is the uncertainties of the dependent variables, and $\sigma_{x_1}$ is the uncertainties of the independent variables. Tables 5 and 6 show the uncertainties of the experimental instrument and the dependent variables, respectively

**Table 5.** Uncertainty of experimental instrument.

| Sensor | Number | Variable Measured | Model | Uncertainty |
|---|---|---|---|---|
| Thermocouple | 8 | Wall temperature | K-type | 0.2% |
| Digital pressure sensor | 2 | Local pressure | Huba Control | 0.1% |
| Flow meter | 1 | Volumetric flow rate | ZYIA Rotameter | 2.0% |
| Temperatures probe | 2 | Bulk temperature | K-type thermocouple with probe | 0.2% |
| Digital multimeter | 1 | Current of the electric heater | UNI-T Multimeter | 0.1% |

The experimental data of $Nu$, $f$ and $\eta$ are provided in Supplementary Materials. Figure 14 illustrates the mechanism of the fluid flow inside the tube for various inserts. The figure emphasizes

the differences in terms of the velocity streamlines, the temperature distribution and the turbulent kinetic energy among four conditions. The comparisons are conducted for a 1% SiC/Water nanofluid that is flowing through a tube that is equipped with various types of inserts with Re equal to 10,000. The plain tube creates a straight path of the velocity streamline, while the presence of inserts creates a helical flow around the inserts, which is also known as a swirl flow. TT with constant PR generates a constant swirl flow along the tube, while IPR and DPR yield stronger flows at the inlet and outlet, respectively. The formation of a fluid flow from the inner tube to the tube wall is visualized in the velocity vector image over cross-sectional plane XY of the tube. According to the velocity vector image, TT IPR yields the densest velocity vector field near the tube wall among the considered inserts; hence, TT IPR creates the largest temperature disruption near the wall region among the geometries. The temperature contours showed that the presence of TT disrupts the temperature gradient in the tube, which results in the reduction of the temperature boundary layer thickness near the wall region. According to the turbulent kinetic energy image, the tubes that are equipped with twisted tapes (PR2, IPR and DPR) show significant differences in their fluid energy contours compared to the plain tube. TT IPR showed fewer contours in TKE; hence, the energy is well dispersed from the tube wall towards the centre of the tube. This is also due to better fluid mixing, which can result in a higher heat transfer rate. However, the twisted tape inserts can create a higher-pressure gradient along the flow direction due to an abrupt change in velocity, which causes higher flow resistance. Using a constant PR (TT PR2) caused higher $\Delta P$ to occur along the tube due to increased tangential contact between the fluid and the tube surface. However, using TT with increasing and decreasing PR (IPR and DPR) can reduce the tangential contact, thereby resulting in a smaller pressure drop. Figure 15 shows the pressure drop across the tube.

**Table 6.** Uncertainty of dependent variables.

| Dependent Variables | Uncertainty |
|---|---|
| *Nu* | ±3.99 |
| *Re* | ±4.13 |
| *f* | ±5.21 |
| $\eta$ | ±6.66 |

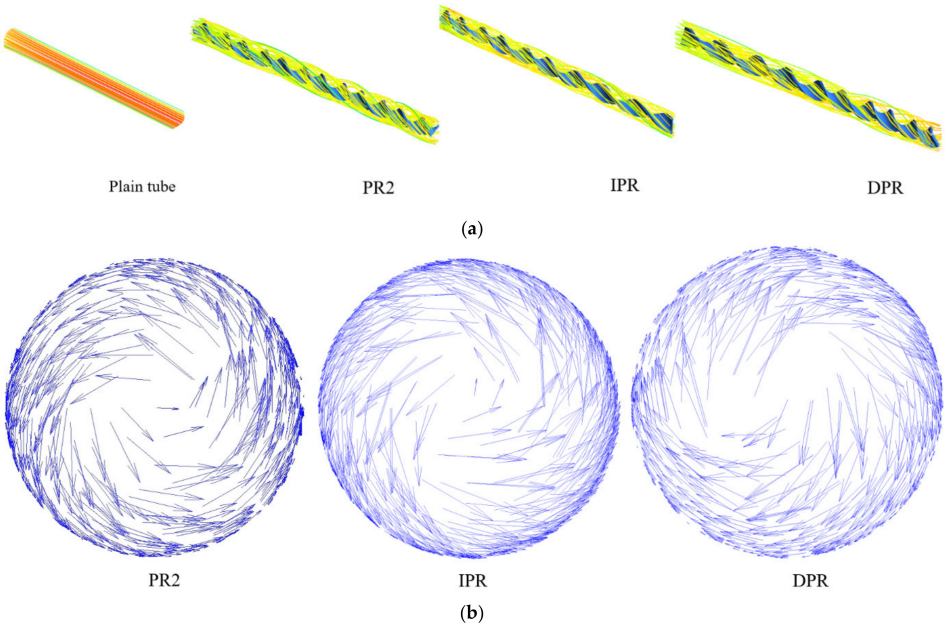


**Figure 14.** *Cont.*

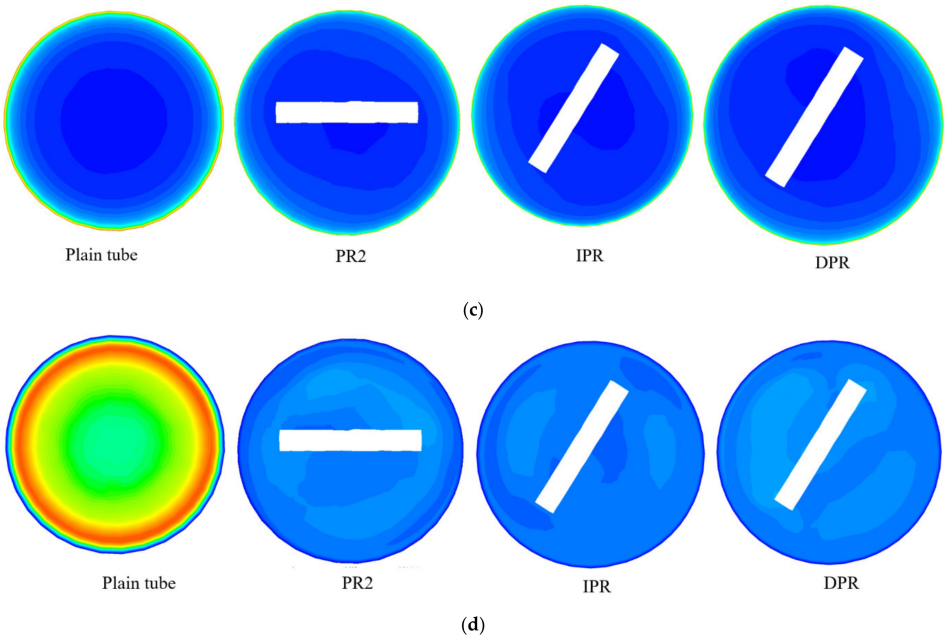


**Figure 14.** (**a**) The velocity streamlines, (**b**) velocity vectors, (**c**) temperature contours, and (**d**) turbulent kinetic energy of a nanofluid that is flowing inside a tube.

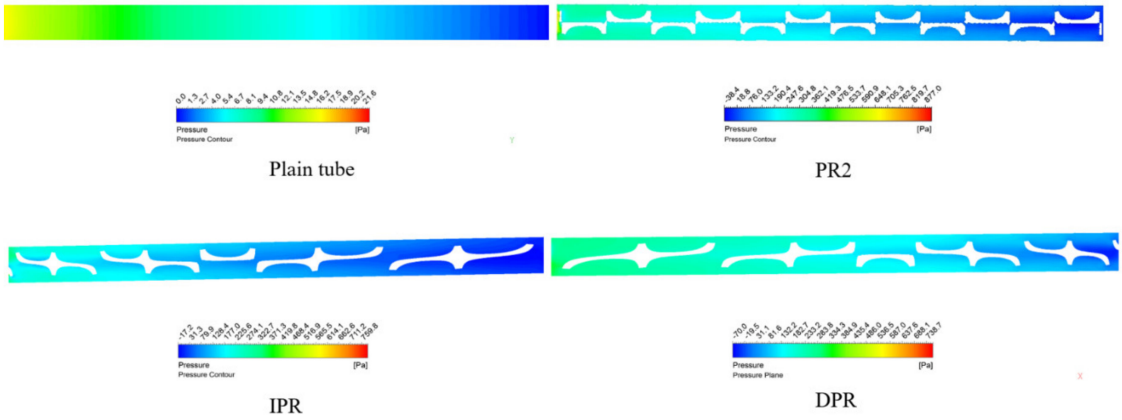


**Figure 15.** Pressure contours across the tube.

Figures 16 and 17 plot the effects of the twisted tape designs for the 1% SiC/Water nanofluid on *Nu* using the numerical and experimental method respectively. *Nu* increases with increasing *Re* for all conditions. At lower *Re* (4000–6000), TT PR2 shows the largest *Nu* values, while at higher *Re*, TT IPR shows the largest *Nu* values. At lower *Re*, TT PR2 creates a constant strong swirl flow across the tube, which can result in better fluid mixing and more efficient thermal boundary layer disruption compared to other TTs. However, at higher *Re*, where fluid is having higher vorticity and the eddy turbulence is dominant, TT IPR can create a more uniform turbulence intensity inside the tube, which leads to higher heat transfer rate across the tube and results in larger *Nu* values [45]. As the fluid approaches the outlet region for TT IPR, the turbulence intensity is slightly reduced due to the gradually increasing PR. However, the intensity drop is small compared to the higher heat transport performance that it offers. The addition of inserts into the tube will cause additional resistance to the fluid flow, which can result in a higher ΔP, which is due to the generation of a larger contact surface by the flow and the surfaces of the inserts. The average deviations between numerical and experimental results for TT PR2, TT IPR and TT DPR are approximately 9.8%, 9.1% and 9.7%, respectively. Figures 18 and 19 plot the variation of $f$ with *Re* at various conditions of the inserts using the numerical and experimental method

respectively. The tube that is equipped with TT IPR yields the lowest $f$ values, followed by TT PR2 and TT DPR due to lower PR near the outlets of the inserts, which creates a smaller fluid-insert contact area and results in less fluid friction. The average deviations between numerical and experimental results of $f$ for TT PR2, TT IPR and TT DPR are approximately 2.1%, 1.9% and 2.4%, respectively. Based on Figures 20 and 21, at a similar condition (1% SiC/Water nanofluid), TT IPR shows the highest $\eta$, followed by TT PR2 and TT DPR. TT IPR yields lower PR at the inlet, which gradually increases near the outlet, thereby resulting in stronger swirling flow near the inlet region, which slightly weakens as it approaches the outlet. However, the lower intensity of the turbulence is countered by a smaller pressure drop near the outlet, which is due to the lower fluid friction (higher PR), which results in larger $\eta$ for the TT IPR geometry.

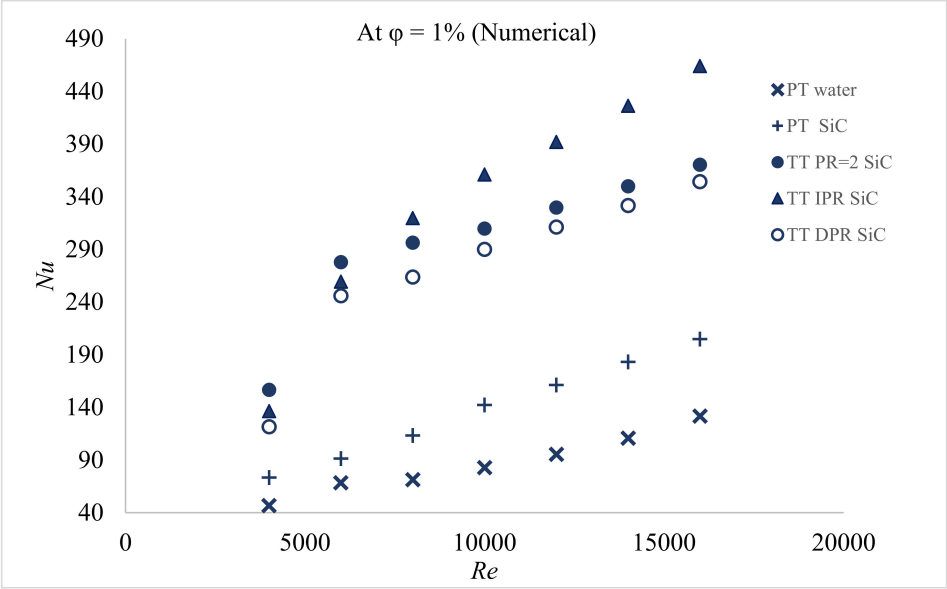


**Figure 16.** Effect of the type of inserts on Nu (Numerical).

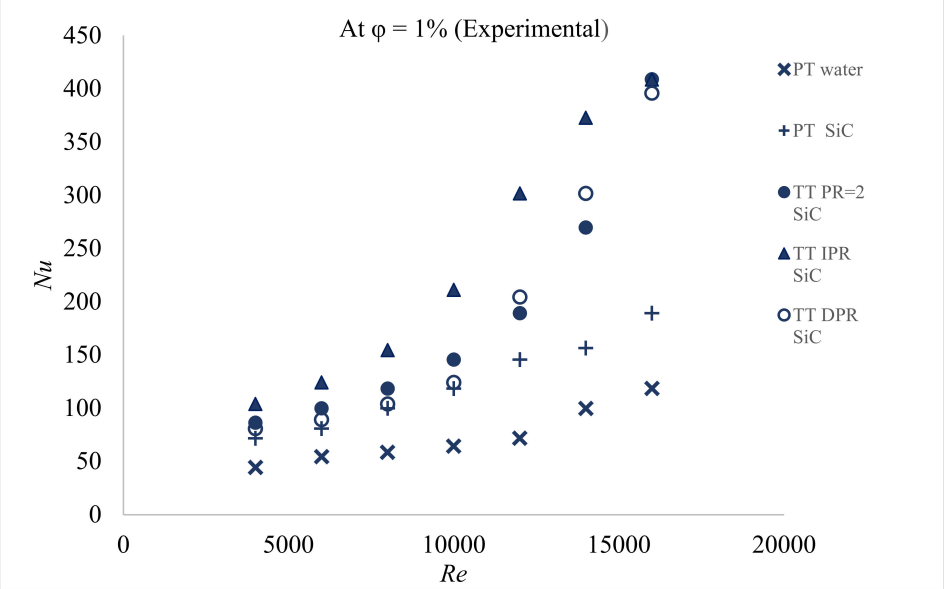


**Figure 17.** Effect of the type of inserts on Nu (Experimental).

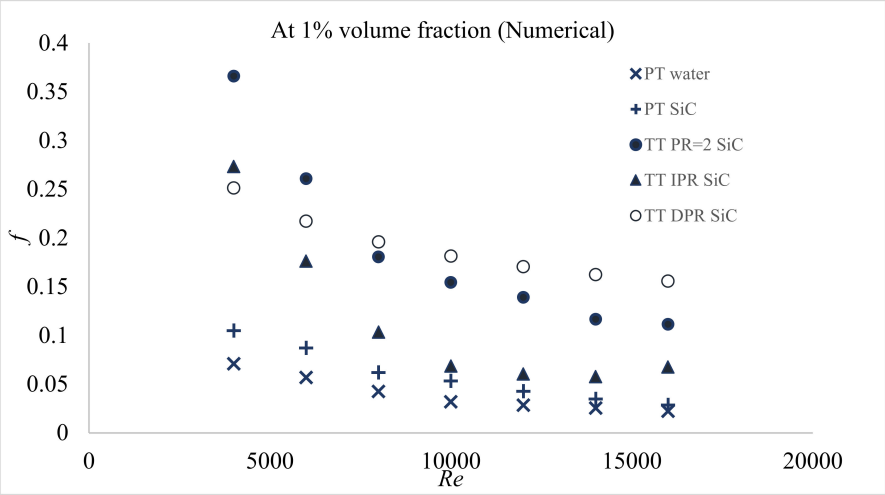


**Figure 18.** Effect of the type of inserts on f (Numerical).

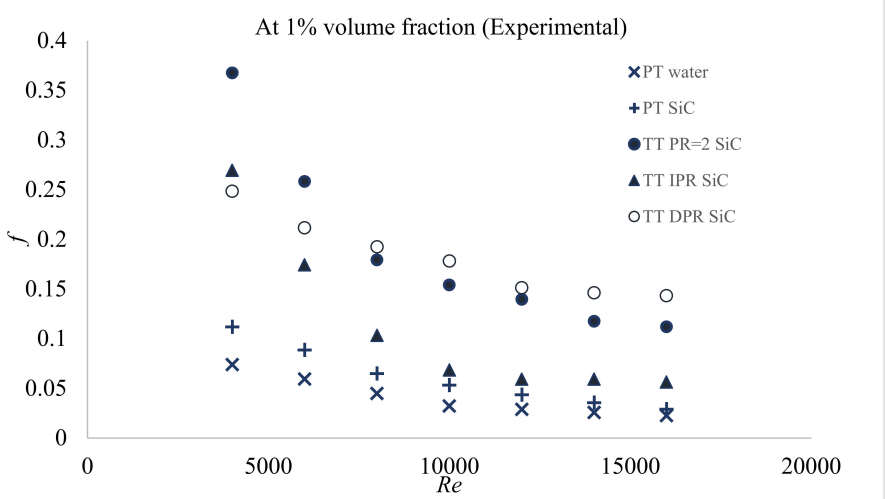


**Figure 19.** Effect of the type of inserts on f (Experimental).

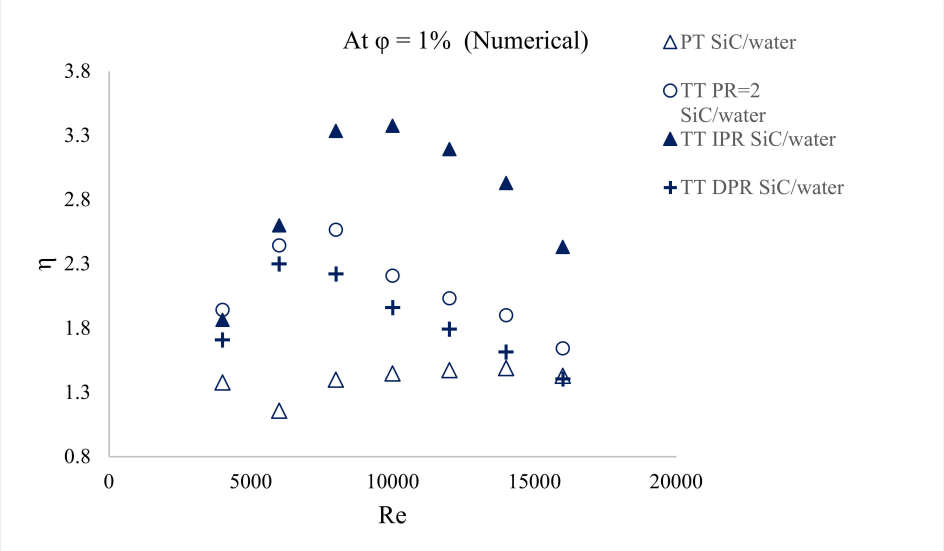


**Figure 20.** Effect of type of inserts on the overall enhancement ratio, η (Numerical).

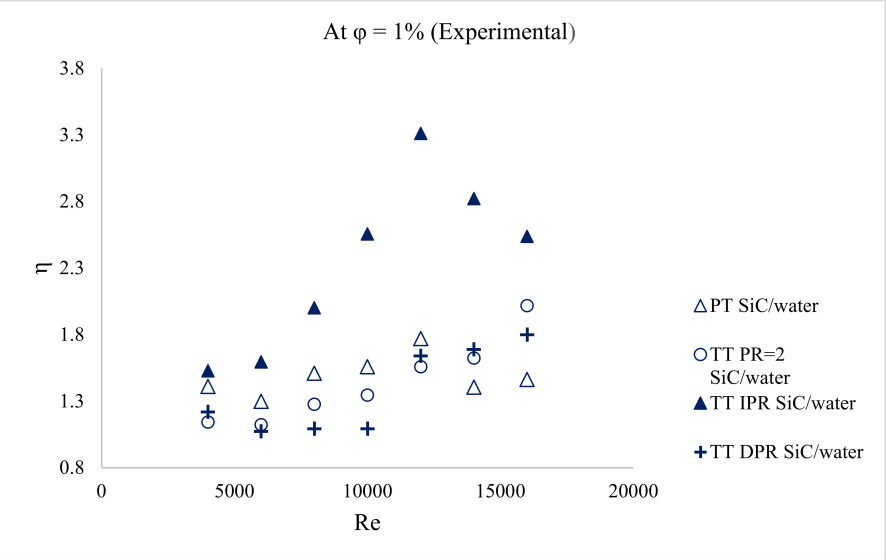


**Figure 21.** Effect of type of inserts on the overall enhancement ratio, η (Experimental)

In addition to the geometry of the inserts, the type of nanofluid is a parameter that is considered in the analysis. Figure 22 illustrates the variations of *Nu* with *Re* for the SiC/Water and $Al_2O_3$/Water nanofluids at 1% $\varphi$ that are flowing inside a circular tube that is equipped with TT IPR. The graphs illustrate that the SiC/Water and $Al_2O_3$/Water nanofluids show similar increasing trends in the *Nu*. SiC/Water nanofluid yields a slightly larger value compared to $Al_2O_3$/Water. The SiC/Water nanofluid has a larger value of *k* than the $Al_2O_3$/Water nanofluid, which contributes to higher *Nu*. The *Nu* values obtained using the numerical method are higher compared to the experimental method due to uncertainties from experimental instruments. Figure 23 illustrates the variation of *f* with Re for SiC/Water $Al_2O_3$/Water nanofluids at similar conditions. The graphs show decreasing trends in *f* values with increasing *Re*. SiC/Water nanofluid creates a slightly higher $\Delta P$ at lower *Re* but shows almost the same value at higher *Re*. Hence, the SiC/Water nanofluid shows a slightly larger value of $\eta$ compared to that of $Al_2O_3$/Water. However, the type of nanoparticles does not have a substantial effect on $\eta$ due to small difference in nanoparticles thermal properties [46], in contrast to other parameters such as the geometry of the inserts and $\varphi$. Hence, further analysis is conducted on parameter $\varphi$.

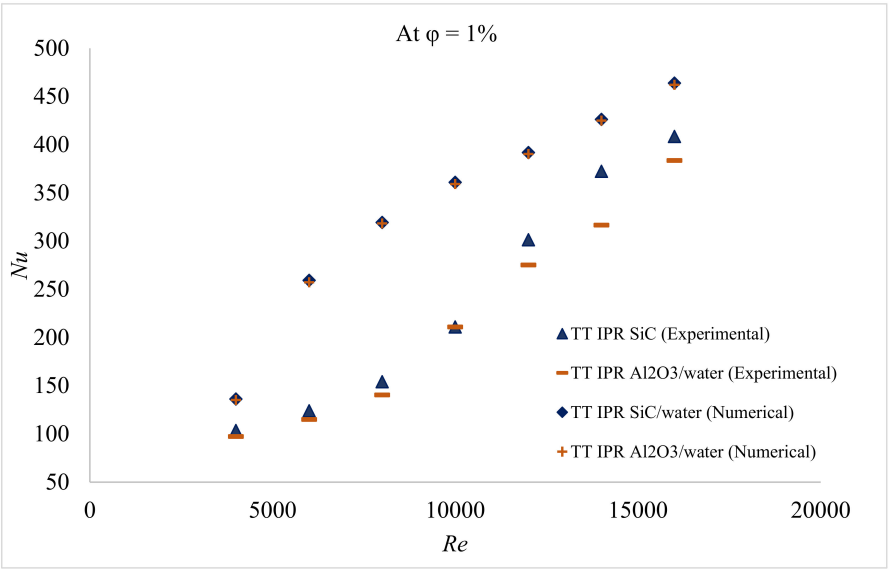


**Figure 22.** Effects of the type of nanoparticles on Nu.

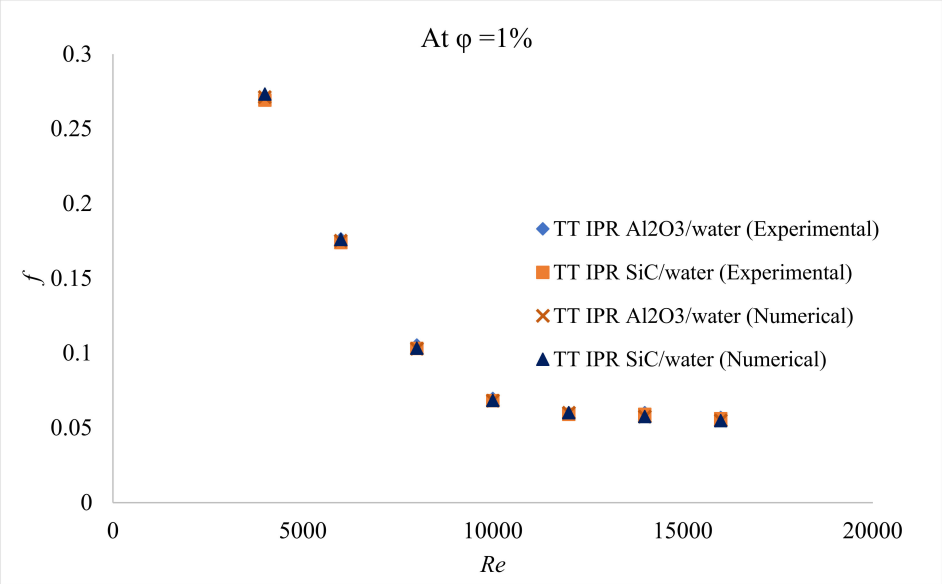


**Figure 23.** Effects of the type of nanoparticles on Nu and f.

Figures 24 and 25 plot the variation of $Nu$ with increasing $Re$ at various values of $\varphi$ for the SiC/Water nanofluid that is flowing inside a smooth tube that is equipped with TT IPR using numerical and experimental methods, respectively. The average deviations between numerical and experimental results for 1% SiC/Water, 2% SiC/Water and 3% SiC/Water are approximately 6.8%, 7.1% and 6.5%, respectively. $Nu$ increases with increasing $\varphi$ (1–3%). This is because the higher concentration of nanoparticles inside the fluid yields a higher thermal conductivity and the drastic movement of the nanoparticles can enhance the heat transfer performance of the system. However, the higher concentration of nanoparticles can lead to a higher $\Delta P$ (referring to Figures 26 and 27), where 3% volume fraction produces a higher pressure drop, which is due to the higher viscosity of the fluid. Hence, selecting the optimal value of $\varphi$ is highly important for ensuring that the largest value of $\eta$ is attained. The average deviations between numerical and experimental results of $f$ for 1% SiC/Water, 2% SiC/Water and 3% SiC/Water approximately are 3.9%, 4.3% and 4.8%, respectively. Figures 28 and 29 illustrate the effect of $\varphi$ to the $\eta$. The highest value of $\eta$ is obtained for SiC/Water nanofluid at $\varphi$, *which* equals to 3% with the range of $Re$ from 10,000 to 12,000.

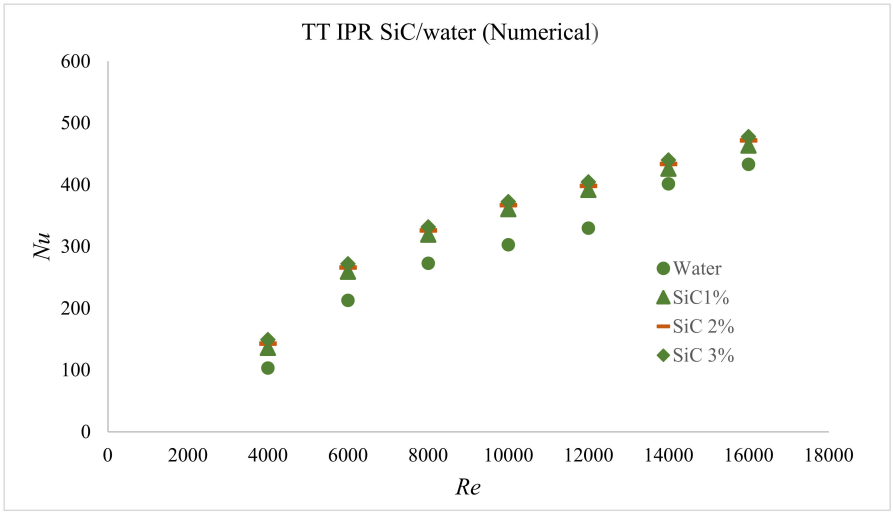


**Figure 24.** Effect of the nanofluid volume fraction φ on Nu (Numerical).

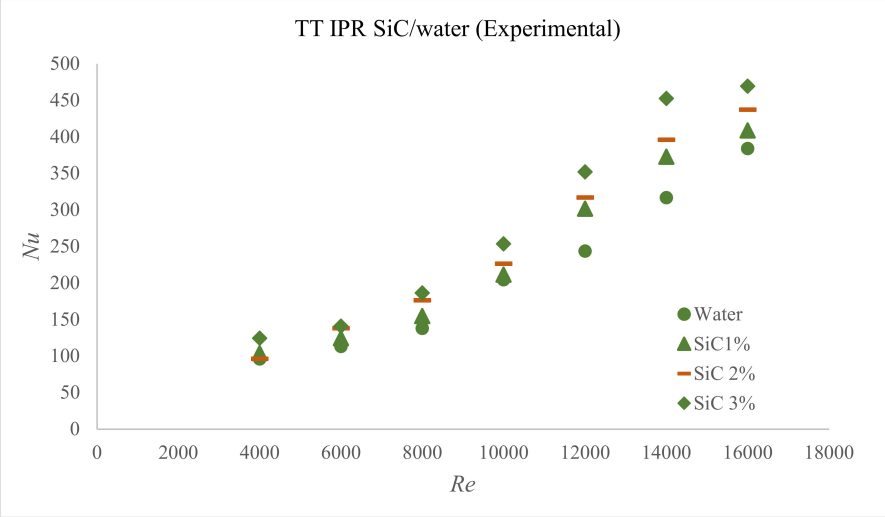


**Figure 25.** Effect of the nanofluid volume fraction φ on Nu (Experimental).

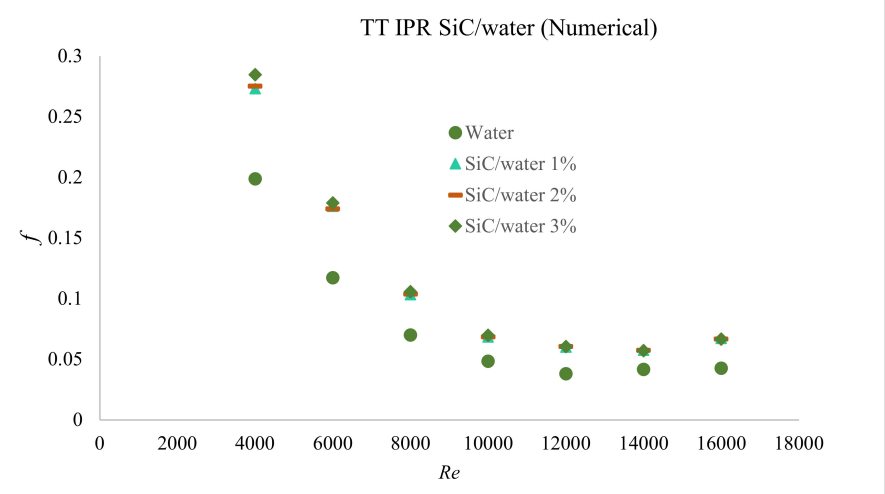


**Figure 26.** Effect of the nanofluid volume fraction φ on f. (Numerical).

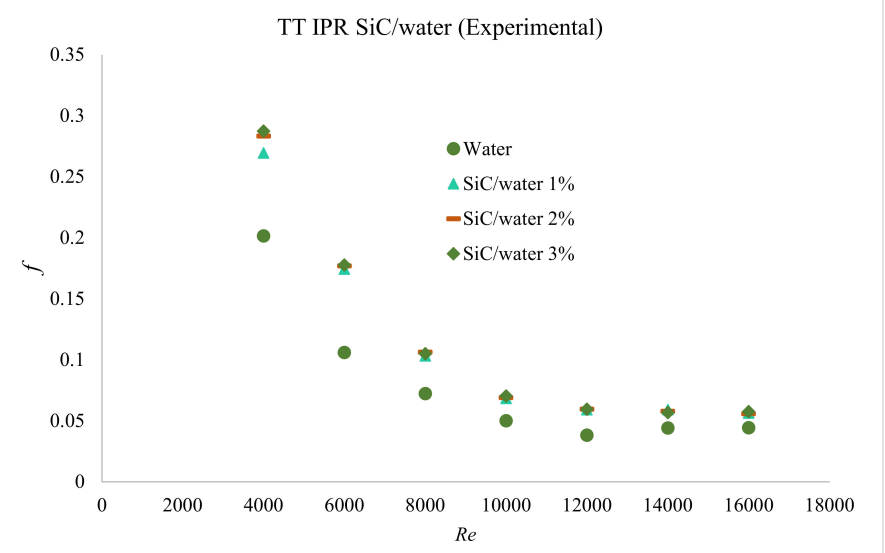


**Figure 27.** Effect of the nanofluid volume fraction φ on f (Experimental).

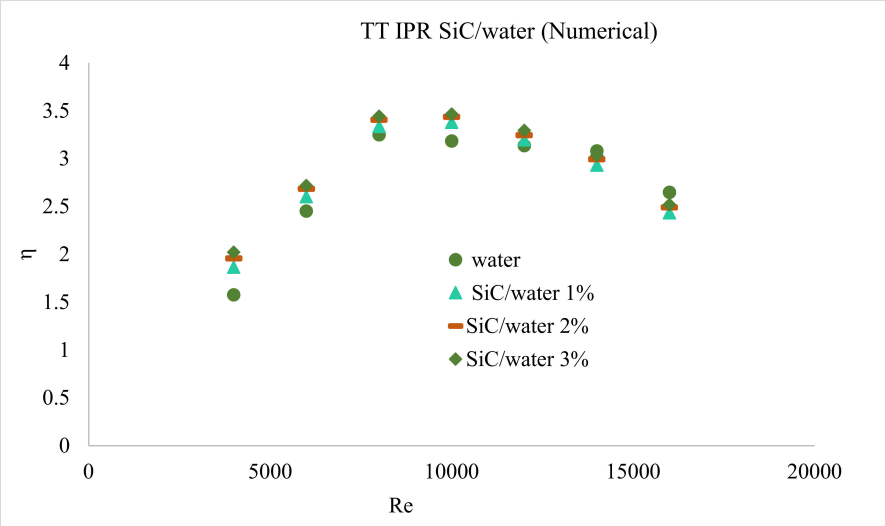


**Figure 28.** Effect of the nanofluid volume fraction φ on η (Numerical).

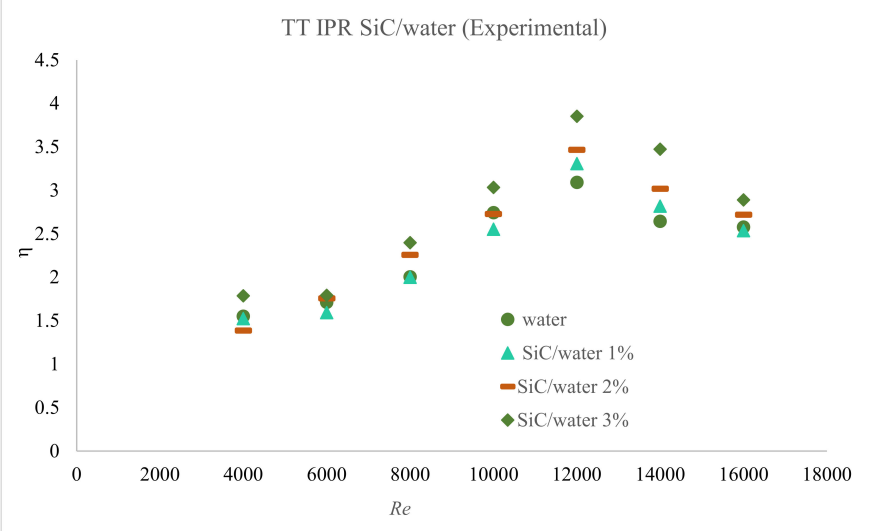


**Figure 29.** Effect of the nanofluid volume fraction φ on η (Experimental).

## 4. Conclusions

In this study, $Nu$, $f$ and $\eta$ of SIC/Water and $Al_2O_3$/Water nanofluids that are flowing inside a circular tube with twisted tape inserts (TTPR2, TT IPR and TT DPR) are presented. The main conclusions from the analysis are as follows:

- Utilizing TT IPR inside a tube able to manipulate the fluid flow path inside the tube and create a higher swirl flow intensity that improves the heat transfer rate.
- TT IPR having dynamic PR (lower at the inlet) caused higher secondary flow vortexes at the inlet while higher PR to the outlet contributes to lower $f$ towards the outlet of the tube, which eventually results in improvement in $\eta$. The value of $\eta$ is improved up to 10% with the use of SiC/Water nanofluid compared to using TT IPR alone.
- All $Nu$ values increase with increasing $Re$ for all modifications (TT IPR TT DPR and TT PR 2). However, the impact of changing $Re$ is more significant for TT IPR as compared to TT DPR and TT PR 2, especially at Re > 10,000.
- For all modifications of the twisted tape, the values of $Nu$, $f$ and $\eta$ is increased with increasing $\varphi$ from 1% to 3%. Increasing the value of $\varphi$ shows a maximum increase up to ~23.7%, ~10% and 15% of $Nu$, $f$ and $\eta$ respectively as compared to water.

- Using TT IPR inserts enhanced $\eta$ by ~62.2% compared to the plain tube, while increasing $\varphi$ of the SiC/Water nanofluid up to 3% enhanced $\eta$ by 31.6%. This demonstrates that the use of inserts has a more significant effect on the thermal efficiency of the system than using a nanofluid as the working fluid. However, the simultaneous use of these two passive methods increased $\eta$ up to 71.14% compared with using a plain tube with water as the working fluid.
- Utilization of twisted tape with dynamic PR (TT IPR) gives 50% higher $\eta$ compared to constant PR (TT PR2) at the same value of $\varphi$. Hence, this new geometry is the best choice for enhancement in $\eta$ for the heat exchanger device.

*Future Recommendations*

In the future, a thorough experimental study must be conducted to better compare and evaluate the simulation result for example upgrading the current experimental rig by using a sensor with better accuracy and using a chiller to keep the inlet temperature constant. Dynamic PR twisted tape is proven to be good geometry for heat transfer enhancement. Hence, a thorough study into this geometry including finding the optimum value for the progression rate of PR is important for future research. In addition, nanoparticles will tend to create agglomerations within a limited period of time. Hence, the preservation of the stability of the nanofluid is crucial and should be considered in the future.

**Supplementary Materials:** The following are available online at http://www.mdpi.com/1996-1073/13/8/2095/s1, Table S1: Experimental data of *Nu*, Table S2: Experimental data of $\Delta P$, Table S3: Experimental data of *f*, Table S4: Experimental data of $Nu/Nu_p$, Table S5: Experimental data of $f/f_p$, Table S6: Experimental data of $\eta$.

**Author Contributions:** Conceptualization, S.A. (Saadah Ahmad) and K.S.; methodology, S.A. (Saadah Ahmad); software, S.A. (Saadah Ahmad) and S.A. (Shahrir Abdullah); validation, S.A. (Saadah Ahmad); formal analysis, S.A. (Saadah Ahmad); investigation, S.A. (Saadah Ahmad); resources, S.A. (Saadah Ahmad); data curation, S.A. (Saadah Ahmad); writing—original draft preparation, S.A. (Saadah Ahmad); writing—review and editing, S.A. (Saadah Ahmad); visualization, S.A. (Saadah Ahmad); supervision, S.A. (Shahrir Abdullah) and K.S.; project administration, S.A. (Shahrir Abdullah); funding acquisition, K.S. All authors have read and agreed to the published version of the manuscript.

**Funding:** This research was funded by Universiti Kebangsaan Malaysia, grant number DIP-2019-019 and FRGS/1/2019/TK07/UKM/01/3.

**Acknowledgments:** The authors would like to thank to the Universiti Kebangsaan Malaysia for the use of its laboratory facilities.

**Conflicts of Interest:** The authors declare no conflict of interest.

## Nomenclature

| | |
|---|---|
| $Al_2O_3$. | Aluminum Oxide |
| $c_p$ | Specific Heat |
| D | Tube diameter |
| k | Thermal conductivity |
| L | Tube Length |
| Nu | Nusselt number |
| PR | Pitch Ratio |
| $\Delta P$ | Pressure drop |
| Re | Reynolds number |
| RNG | Renormalized group |
| SiC | Silica oxide |
| t | Twisted tape thickness |
| $T_f$ | Bulk temperature |
| $T_{in}$ | Inlet temperature |
| $T_w$ | Pipe wall temperature |
| TT DPR | Constant-Decreased pitch ratio twisted tape |
| TT IPR | Constant-Increased pitch ratio twisted tape |
| TT PR2 | Twisted tape with pitch ratio 2 |

| | |
|---|---|
| w | Twisted tape width |
| y | Pitch Length |
| $\eta$ | Overall Enhancement Ratio |
| $\varphi$ | Nanoparticles Volume Fraction |
| $\rho$ | Density |
| $\mu$ | Viscosity |

## References


1. Ajeel, R.K.; Salim, W.S.-I.; Sopian, K.; Yusoff, M.Z.; Hasnan, K.; Ibrahim, A.; Al-Waeli, A.H.A. Turbulent convective heat transfer of silica oxide nanofluid through corrugated channels: An experimental and numerical study. *Int. J. Heat Mass Transf.* **2019**, *145*, 118806. [CrossRef]
2. Abed, A.M.; Alghoul, M.A.; Sopian, K.; Mohammed, H.A.; Majdi, H.S.; Al-Shamani, A.N. Design characteristics of corrugated trapezoidal plate heat exchangers using nanofluids. *Chem. Eng. Process. Process Intensif.* **2015**, *87*, 88–103. [CrossRef]
3. Eiamsa-Ard, S.; Promvonge, P. Thermal characteristics in round tube fitted with serrated twisted tape. *Appl. Therm. Eng.* **2010**, *30*, 1673–1682. [CrossRef]
4. Piriyarungrod, N.; Kumar, M.; Thianpong, C.; Pimsarn, M.; Chuwattanakul, V.; Eiamsa-Ard, S.; Chuwattabakul, V. Intensification of thermo-hydraulic performance in heat exchanger tube inserted with multiple twisted-tapes. *Appl. Therm. Eng.* **2018**, *136*, 516–530. [CrossRef]
5. Saravanan, A.; Senthilkumaar, J.; Jaisankar, S. Performance assessment in V-trough solar water heater fitted with square and V-cut twisted tape inserts. *Appl. Therm. Eng.* **2016**, *102*, 476–486. [CrossRef]
6. Liu, G.; Yang, C.; Zhang, J.; Zong, H.; Xu, B.; Qian, J.-Y. Internal Flow Analysis of a Heat Transfer Enhanced Tube with a Segmented Twisted Tape Insert. *Energies* **2020**, *13*, 207. [CrossRef]
7. Zhang, S.; Lu, L.; Dong, C.; Hyun, S. Performance evaluation of a double-pipe heat exchanger fi tted with self- rotating twisted tapes. *Appl. Therm. Eng.* **2019**, *158*, 113770. [CrossRef]
8. Nakhchi, M.; Esfahani, J. Cu-water nanofluid flow and heat transfer in a heat exchanger tube equipped with cross-cut twisted tape. *Powder Technol.* **2018**, *339*, 985–994. [CrossRef]
9. Salman, S.D.; Kadhum, A.A.H.; Takriff, M.S.; Mohamad, A.B. CFD Simulation of Heat Transfer Augmentation in a Circular Tube Fitted with Alternative Axis Twisted Tape in Laminar Flow under a Constant Heat Flux. *Heat Transf. Res.* **2014**, *43*, 384–396. [CrossRef]
10. Bahiraei, M.; Mazaheri, N.; Hassanzamani, S.M. Efficacy of a new graphene–platinum nanofluid in tubes fitted with single and twin twisted tapes regarding counter and co-swirling flows for efficient use of energy. *Int. J. Mech. Sci.* **2019**, *150*, 290–303. [CrossRef]
11. Eiamsa-ard, S.; Kiatkittipong, K.; Jedsadaratanachai, W. Heat transfer enhancement of TiO2/Water nanofluid in a heat exchanger tube equipped with overlapped dual twisted-tapes. *Eng. Sci. Technol. Int. J.* **2015**, *18*, 336–350. [CrossRef]
12. Li, Z.; Sheikholeslami, M.; Jafaryar, M.; Shafee, A.; Chamkha, A.J. Investigation of nanofluid entropy generation in a heat exchanger with helical twisted tapes. *J. Mol. Liq.* **2018**, *266*, 797–805. [CrossRef]
13. Zheng, L.; Xie, Y.; Zhang, D. Numerical investigation on heat transfer performance and flow characteristics in circular tubes with dimpled twisted tapes using Al 2 O 3-water nanofluid. *Int. J. Heat Mass Transf.* **2017**, *111*, 962–981. [CrossRef]
14. Safikhani, H.; Abbasi, F. Numerical study of nanofluid flow in flat tubes fitted with multiple twisted tapes. *Adv. Powder Technol.* **2015**, *26*, 1609–1617. [CrossRef]
15. Gnanavel, C.; Saravanan, R.; Chandrasekaran, M. Materials Today: Proceedings Heat transfer enhancement through nano-fluids and twisted tape insert with rectangular cut on its rib in a double pipe heat exchanger. *Mater. Today Proc.* **2019**.
16. Maddah, H.; Alizadeh, M.; Ghasemi, N.; Rafidah, S.; Alwi, W. Experimental study of Al $2O_3$/Water nanofluid turbulent heat transfer enhancement in the horizontal double pipes fitted with modified twisted tapes. *Int. J. Heat Mass Transf.* **2014**, *78*, 1042–1054. [CrossRef]
17. Khoshvaght-aliabadi, M.; Davoudi, S.; Dibaei, M.H. Chemical Engineering Research and Design Performance of agitated-vessel U tube heat exchanger using spiky twisted tapes and water based metallic nanofluids. *Chem. Eng. Res. Des.* **2018**, *133*, 26–39. [CrossRef]

18. Murali, G.; Nagendra, B.; Jaya, J. Materials Today: Proceedings CFD analysis on heat transfer and pressure drop characteristics of turbulent flow in a tube fitted with trapezoidal-cut twisted tape insert using $Fe_3O_4$ nano fluid. *Mater. Today Proc.* **2019**.
19. Rahimi, M.; Shabanian, S.R.; Alsairafi, A.A. Experimental and CFD studies on heat transfer and friction factor characteristics of a tube equipped with modified twisted tape inserts. *Chem. Eng. Process. Process. Intensif.* **2009**, *48*, 762–770. [CrossRef]
20. Tabatabaeikia, S.; Mohammed, H.A.; Nik-Ghazali, N.; Shahizare, B. Heat Transfer Enhancement by Using Different Types of Inserts. *Adv. Mech. Eng.* **2014**, *6*, 250354. [CrossRef]
21. Eiamsa-Ard, S.; Pimsarn, M.; Thianpong, C. Performance Assessment in a Heat Exchanger Tube with Opposite/Parallel Wing Twisted Tapes. *Adv. Mech. Eng.* **2014**, *7*, 652536. [CrossRef]
22. Khoshvaght-aliabadi, M.; Eskandari, M. Influence of twist length variations on thermal—Hydraulic specifications of twisted-tape inserts in presence of Cu – water nanofluid. *Exp. Therm. Fluid Sci.* **2015**, *61*, 230–240. [CrossRef]
23. Qi, C.; Wang, G.; Yan, Y.Y.; Mei, S.; Luo, T. Effect of rotating twisted tape on thermo-hydraulic performances of nanofluids in heat-exchanger systems. *Energy Convers. Manag.* **2018**, *166*, 744–757. [CrossRef]
24. Abdullah, M.F.; Zulkifli, R.; Harun, Z.; Abdullah, S.; Wan Ghopa, W.A.; Najm, A.S.; Sulaiman, N.H. Impact of the TiO2 nanosolution concentration on heat transfer enhancement of the twin impingement jet of a heated aluminum plate. *Micromachines.* **2019**, *10*, 176. [CrossRef] [PubMed]
25. Chang, T.; Syu, S.; Yang, Y. Effects of particle volume fraction on spray heat transfer performance of Al 2 O 3—Water nanofluid. *Int. J. Heat Mass Transf.* **2012**, *55*, 1014–1021. [CrossRef]
26. Duangthongsuk, W.; Wongwises, S. An experimental study on the heat transfer performance and pressure drop of TiO2-water nanofluids flowing under a turbulent flow regime. *Int. J. Heat Mass Transf.* **2010**, *53*, 334–344. [CrossRef]
27. Vajjha, R.S.; Das, D.K. A review and analysis on influence of temperature and concentration of nanofluids on thermophysical properties, heat transfer and pumping power. *Int. J. Heat Mass Transf.* **2012**, *55*, 4063–4078. [CrossRef]
28. Kane, J.M. Ansys Fluent 12.0 User's Guide. 2009. Available online: https://www.afs.enea.it/project/neptunius/docs/fluent/html/ug/main_pre.htm (accessed on 20 November 2018).
29. Patankar, S.V.; Spalding, D.B.A. A calculation procedure for heat, mass and momentum transfer in three-dimensional parabolic flows. *Int. J. Heat Mass Transf.* **1972**, *15*, 1787–1806. [CrossRef]
30. Godson, L.; Raja, B.; Lal, D.M.; Wongwises, S. Enhancement of heat transfer using nanofluids—An overview. *Renew. Sustain. Energy Rev.* **2010**, *14*, 629–641. [CrossRef]
31. Ebrahimi, A.; Rikhtegar, F.; Sabaghan, A.; Roohi, E. Heat transfer and entropy generation in a microchannel with longitudinal vortex generators using nanofluids. *Energy* **2016**, *101*, 190–201. [CrossRef]
32. Mahian, O.; Kolsi, L.; Amani, M.; Estellé, P.; Ahmadi, G.; Kleinstreuer, C.; Marshall, J.S.; Siavashi, M.; Izadgoshasb, I.; Niazmand, H.; et al. Recent advances in modeling and simulation of nanofluid flows-Part I: Fundamentals and theory. *Phys. Rep.* **2019**, *790*, 1–48. [CrossRef]
33. Hamilton, R.L.; Crosser, O.K. Thermal Conductivity of Heterogeneous Two-Component Systems. *Ind. Eng. Chem. Fundam.* **1962**, *1*, 187–191. [CrossRef]
34. Zhou, S.-Q.; Ni, R. Measurement of the specific heat capacity of water-based Al[sub 2]O[sub 3] nanofluid. *Appl. Phys. Lett.* **2008**, *92*, 93123. [CrossRef]
35. Brinkman, H.C. The Viscosity of Concentrated Suspensions and Solutions. *J. Chem. Phys.* **1952**, *20*, 571. [CrossRef]
36. Maxwell, J.C. *A Treatise on Electricity and Magnetism*, 2nd ed.; Oxford University Press: Oxford, UK, 1904.
37. Ramakumar, B.V.N.; Arsha, J.D.; Tayal, P. Tapered Twisted Tape Inserts for Enhanced Heat Transfer. *J. Heat Transf.* **2015**, *138*, 011901. [CrossRef]
38. Incropera, F.P.; DeWitt, D.P.; Bergman, T.L.; Lavine, A.S. *Fundamentals of Heat and Mass Transfer*; John-Wiley & Sons: Hoboken, NJ, USA, 2006.
39. Eiamsa-Ard, S.; Kiatkittipong, K. Heat transfer enhancement by multiple twisted tape inserts and $TiO_2$/Water nanofluid. *Appl. Therm. Eng.* **2014**, *70*, 896–924. [CrossRef]
40. Karami, A.; Rezaei, E.; Shahhosseni, M.; Aghakhani, M. Optimization of heat transfer in an air cooler equipped with classic twisted tape inserts using imperialist competitive algorithm. *Exp. Therm. Fluid Sci.* **2012**, *38*, 195–200. [CrossRef]

41. Naphon, P. Heat transfer and pressure drop in the horizontal double pipes with and without twisted tape insert. *Int. Commun. Heat Mass Transf.* **2006**, *33*, 166–175. [CrossRef]
42. Manglik, R.M.; Bergles, A.E. Heat Transfer and Pressure Drop Correlations for Twisted-Tape Inserts in Isothermal Tubes: Part II—Transition and Turbulent Flows. *J. Heat Transf.* **1993**, *115*, 890–896. [CrossRef]
43. Ponnada, S.; Subrahmanyam, T.; Naidu, S.V. A comparative study on the thermal performance of water in a circular tube with twisted tapes, perforated twisted tapes and perforated twisted tapes with alternate axis. **2018**, *136*, 530–538. [CrossRef]
44. Moffat, R.J. Describing the uncertainties in experimental results. *Exp. Therm. Fluid Sci.* **1988**, *1*, 3–17. [CrossRef]
45. Van Buren, S.; Miranda, A.C.; Polifke, W. Large eddy simulation of enhanced heat transfer in pulsatile turbulent channel flow. *Int. J. Heat Mass Transf.* **2019**, *144*, 118585. [CrossRef]
46. Leong, K.Y.; K. Z. Ku Ahmad, K.Z.; Ong, H.C.; Ghazali, M.J.; Baharum, A. Synthesis and thermal conductivity characteristic of hybrid nanofluids—A review. *Renew. Sustain. Energy Rev.* **2017**, *75*, 868–878. [CrossRef]